ADVANCED FUNCTIONAL MATERIALS
www.afm-journal.de

Materials Views
www.MaterialsViews.com

Compositional and Morphological Studies of Polythiophene/Polyfluorene Blends in Inverted Architecture Hybrid Solar Cells

*Yana Vaynzof, Thomas J. K. Brenner, Dinesh Kabra, Henning Sirringhaus, and Richard H. Friend**

This work investigates the composition and morphology of films of poly(3-hexylthiophene) (P3HT), polyfluorene co-polymer poly((9,9-dioctylfluorene)-2,7-diyl-alt-[4,7-bis(3-hexylthien-5-yl)-2,1,3-benzothiadiazole]-2′,2″-diyl) (F8TBT) and blends thereof that are used in efficient all-polymer solar cells. Ultraviolet photoemission spectroscopy (UPS) and X-ray photoemission spectroscopy (XPS) studies on thin polymer and blend films on ZnO substrates reveal the existence of a 1–2 nm thick P3HT layer at the top surface of the blend films. XPS depth profiling studies reveal a density wave ($\lambda \approx 70$ nm) originating from the air interface. As no preferential accumulation is observed at the bottom interface with ZnO, the composition at this interface is consistent with the original composition of the blend solution prior to spin-coating. The morphology of this buried interface was studied by means of atomic force microscopy (AFM) and revealed that upon annealing the average domain size increases slightly (from 27 nm to 40 nm). It is observed that the photovoltaic performance of such inverted hybrid device improves upon annealing, however we believe this to mostly be a result of increased crystallinity in the P3HT domains leading to improved charge transport in the device, rather than changes in the blend phase separation.

1. Introduction

Almost two decades after their initial demonstration,[1,2] solution-processed conjugated polymer based photovoltaic devices continue to draw a great deal of attention from the scientific community. The vast majority of the reported research focuses on photovoltaic devices the active layer of which is comprised of a blend of a conjugated polymer with fullerene derivatives such as, [6,6]-phenyl-C61-butyric acid methyl ester ([60]PCBM) or [6,6]-Phenyl-C71-butyric acid methyl ester ([70]PCBM).[3–6] In these systems, the conjugated polymer acts as a donor material and the fullerene derivative acts as an acceptor. Alternatively, several attempts have been made to fabricate efficient all-polymer photovoltaic devices. Systems such as poly(9,9-dioctylfluorene-co-bis-N,N-(4-butylphenyl)-bis-N,N-phenyl-1,4-phenylenediamine) (PFB): poly(9,9-dioctylfluorene-co-benzo-thiadiazole) (F8BT),[7] poly(3-hexylthiophene) (P3HT): poly((9,9-dioctylfluorene)-2,7-diyl-alt-[4,7-bis(3-hexylthien-5-yl)-2,1,3-benzothiadiazole]-2′,2″-diyl) (F8TBT),[8] and poly[3-(4-n-octyl)-phenylthiophene] (POPT): poly[2-methoxy-5-(2′-ethylhexyloxy)-1,4-(1-cyanovinylene) phenylene] (CNPPV)[9] have been investigated and power conversion efficiencies (PCE) as high as 2% have been reported. The use of a conjugated polymer as the acceptor material in the bulk heterojunction solar cell offers several advantages over the widely used fullerene derivatives. Firstly, conjugated polymers have higher absorption coefficients over a large range of wavelengths than the fullerene derivatives. Additionally, the flexibility in the design of the energetic position of the lowest unoccupied molecular level (LUMO) allows efficient charge separation in conjunction with high open-circuit voltage (V_{OC}). However, despite these advantages, the performance of all-polymer photovoltaic devices is notably inferior to their polymer:fullerene counterparts. It has been previously reported that the length scale of the phase separated domains has a great impact on the performance of these devices.[10] These length scales are affected by numerous parameters, such as: deposition method,[11] the common solvent[12] or solvent mixture,[13] the molecular weight of the polymers,[14] composition,[7] substrate surface,[15] additives[16] and more. Although attempts have been made to adjust the typical domain size in all-polymer solar cells to increase the device efficiency, achieving good control over the morphology on length scales comparable to the exciton diffusion length still remains a challenge.[17] Therefore, it is crucial to gain understanding of the physical mechanisms driving the phase separation in these systems and learn to control it.

Herein, we present a complete study of the composition and morphology of one of the best performing all-polymer

Dr. Y. Vaynzof, Dr. T. J. K. Brenner,[+] Dr. D. Kabra, Prof. H. Sirringhaus, Prof. Sir R. H. Friend
Cavendish Laboratory
University of Cambridge
JJ Thomson Ave., Cambridge, CB3 0HE, UK
E-mail: rhf10@cam.ac.uk
[+] Current address: Max Planck Institute for the Science of Light, Günther-Scharowsky-Straße 1, 90762 Erlangen, Germany

DOI: 10.1002/adfm.201103008

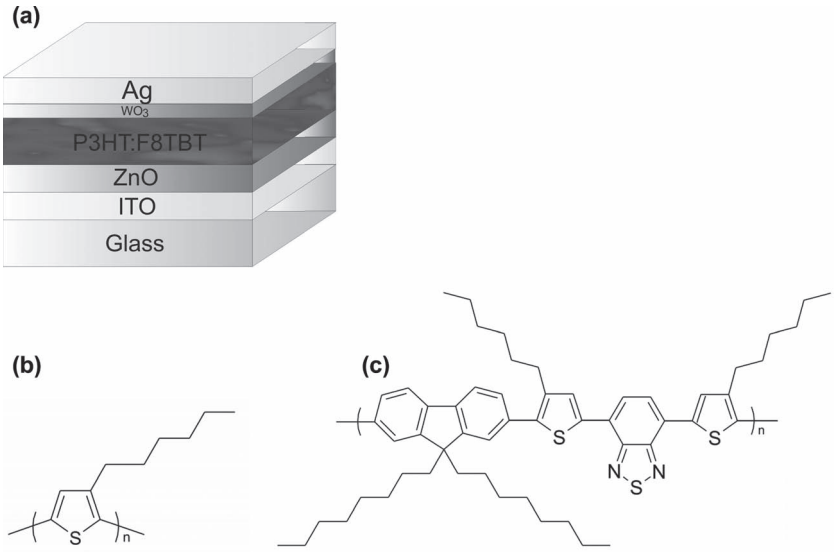

Figure 1. a) Schematic structure of an inverted P3HT:F8TBT photovoltaic device. Chemical structures of b) P3HT and c) F8TBT.

photovoltaic systems, P3HT:F8TBT. The device structure along with the chemical structures of the P3HT and F8TBT polymers are shown in **Figure 1**. The device performance was optimized empirically: using xylene as a solvent and an annealing step at 140 °C for 10 minutes were shown to lead to the best PCE of 1.8%.[18] We follow the empirically optimized fabrication procedure and study the composition and phase separation in the films by means of Ultra violet photoemission spectroscopy (UPS), X-ray photoemission spectroscopy (XPS) and XPS depth profiling. We have recently employed this technique to study the phase separation in P3HT:PCBM blends.[19] Here, in the case of P3HT:F8TBT, we observe a compositional density wave originating from the air surface, however no such wave is detected at the substrate interface, suggesting that it acts as a 'neutral surface'. The wavelength λ of observed density wave is estimated to be 70 nm. Exposing the interface with the substrate and imaging the bottom surface of the polymer blend film by means of Atomic Force Microscopy (AFM) reveals that films annealed at 140 °C show typical domain size of ~40 nm, approximately half of the density wave wavelength. Finally we demonstrate the improved photovoltaic performance of the devices upon annealing at 140 °C, which we interpret to result from improved crystallinity of the P3HT rather than enhanced degree of phase separation, as we measure the typical domain size of unannealed films to be ~30 nm.

2. Results and Discussion

2.1. Composition of P3HT, F8TBT and P3HT:F8TBT thin films

The C1s, S2p and N1s XPS spectra taken on P3HT, F8TBT and P3HT:F8TBT thin films are shown in **Figure 2**. In the case of P3HT, a single S2p doublet is observed at binding energies of 163.9 eV and 165.1 eV, consistent with a S in a thiophene unit. The C1s signal is composed of three C species at 284.8 eV, 284.4 eV and 285.2 eV, corresponding to C–C, C=C and C–S, respectively. As expected, no N1s signal is observed in the P3HT films.

In the S2p spectrum collected on the F8TBT films, we clearly see the contribution from the two species of S in the polymer. The low energy doublet (at binding energy of 164.05 eV) corresponds to the S in the two thiophene units in F8TBT, in agreement with the S doublet previously measured for the thiophene units in P3HT. Whereas the high energy doublet (at binding energy of 165.65 eV) corresponds to the S in the benzothiadiazole (BT) unit of the polymer, consistent with the higher oxidation state of the S in a BT unit. A single peak at a binding energy of 399.45 eV in the N1s spectrum originates from the two N atoms in the BT unit. Accordingly, the C1s signal is decomposed to contributions from C–C, C=C, C–S and C–N.

The measured composition values are in good agreement with the theoretical stochiometric values and are summarized in **Table 1**.

XPS spectra taken on P3HT:F8TBT blend film appear in the bottom row of Figure 2. As the film thickness is similar to the XPS electron escape depth (4–5 nm), the spectra are collected from the entire film thickness and the expected average composition of the P3HT:F8TBT blend is 1:1. The S2p spectra consists of two S doublets (binding energies of 164.1 eV and 165.3 eV), similar to the F8TBT case. It is evident that the contribution from the S originating from the BT unit of the F8TBT is lower than that of the pure polymer film. Similarly the N1s peak (binding energy of 399.45 eV) appears smaller than that in the F8TBT spectrum. The atomic percentage of N in the blend is 49.8% of the value for the pure polymer, in agreement with

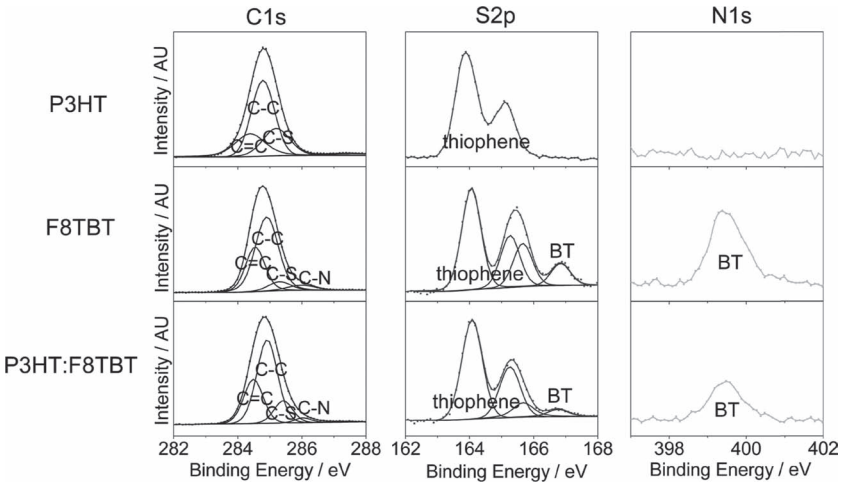

Figure 2. C1s, S2p and N1s XPS spectra taken on P3HT, F8TBT and P3HT:F8TBT thin films.

Table 1. Calculated and measured atomic percentage composition values of C–C, C=C, C–S, C–N, S(thiophene), S(BT) and N chemical species in P3HT, F8TBT and P3HT:F8TBT films. The calculated values were obtained using the ideal polymer structures as depicted in Figure 1.

	P3HT		F8TBT		P3HT:F8TBT	
	Atomic% measured	Atomic% calculated	Atomic% measured	Atomic% calculated	Atomic% measured	Atomic% calculated
C–C	47.57	54.54	54.18	61.66	51.40	57.39
C=C	21.33	18.18	27.27	20.0	25.72	20.00
C–S	21.33	18.18	6.30	6.66	12.26	12.18
C–N	0	0	4.52	3.34	2.40	1.74
S (thiophene)	9.77	9.10	3.61	3.34	5.93	6.09
S(BT)	0	0	1.51	1.66	0.99	0.87
N	0	0	2.61	3.34	1.30	1.73

the 1:1 blend composition. In addition, we observe that the amounts of N measured on F8TBT and P3HT:F8TBT films are consistently lower than the theoretical values by approximately 20%.

Next, we investigate the layer structure of the thin polymer blend films by means of angle resolved X-ray photoelectron spectroscopy (ARXPS). This technique allows the analysis of the vertical composition of thin films in the order of several nm, and offers the advantages of being non-destructive and highly accurate.

As it is schematically illustrated in **Figure 3**e, with increasing sample tilt angle, the XPS spectra are collected from a decreased depth. This results in a lower intensity signal overall, but allows to calculate the atomic concentration percentage at varying depths. The spectra collected at tilt angle of 60° are the most surface sensitive and approach the surface sensitivity of UPS.

Figure 3a, 3b and 3c show the XPS spectra of C1s, S2p and N1s, respectively, collected at sample tilt angles of 0°, 15°, 30°, 45° and 60°. As expected with increasing sample angle the intensity of the collected signal decreases. However, the rate of the decrease differs for each element. Figure 3d shows the evolution of the atomic percentage with increasing sample angle, normalized to the atomic percentage at angle 0°. It is clear that as we probe closer to the top surface (increasing sample angle), the N atomic percentage is significantly decreased. As the sole contribution to the N1s signal is from the F8TBT polymer and almost no N is detected at sample angle of 60°, we conclude that at the top of the blend surface we find nearly pure P3HT. This is also consistent with the observed increase in S atomic percentage.

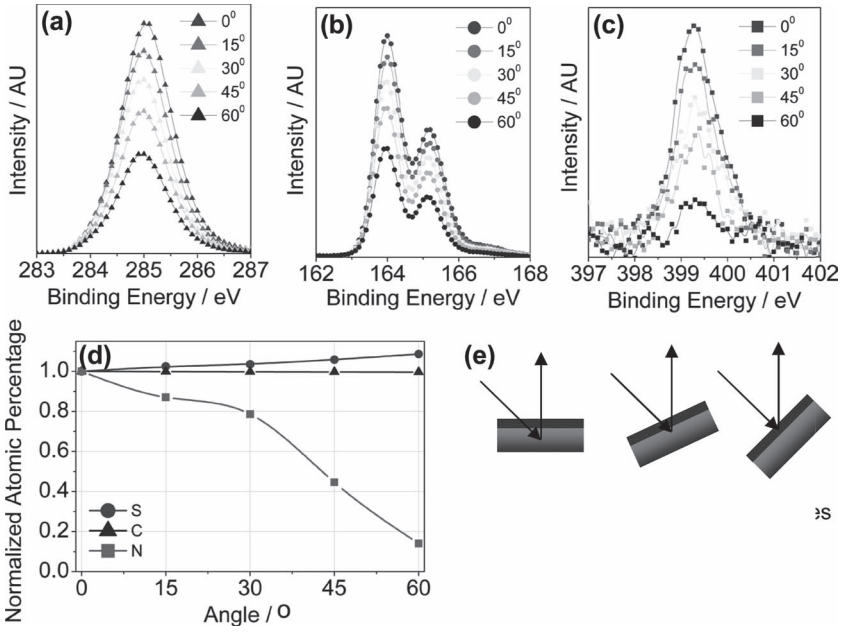

Figure 3. XPS spectra of a) C1s, b) S2p and c) N1s collected at sample angles of 0°, 15°, 30°, 45° and 60°. d) Normalized atomic percentage evolution with increasing sample angle. e) Schematic illustration of the ARXPS technique.

Additionally, we performed UPS measurements on P3HT, F8TBT and P3HT:F8TBT films (**Figure 4**). UPS is much more surface-sensitive than XPS as the photoelectron escape depth is only ~1–2 nm. Traditionally, the low binding energy edge of the polymer valence band corresponds to the position of the highest occupied molecular orbital (HOMO).[20] The energetic difference between the HOMO edge of the P3HT and that of F8TBT is measured to be 0.7 eV, in agreement with what has been previously measured by Friedel et al.[21] using cyclic voltammetry. The UPS spectrum taken on a P3HT:F8TBT blend film is completely dominated by the P3HT features, suggesting that the top ~1–2 nm of the blend film are composed of a pure P3HT layer, in excellent agreement with the ARXPS measurements. This has been previously observed in the case of P3HT:PCBM films and is attributed to the lower surface energy of the P3HT.[22]

McNeill et al.[23] previously observed that the top surface of P3HT:F8TBT films is P3HT rich, in agreement with our measurements.

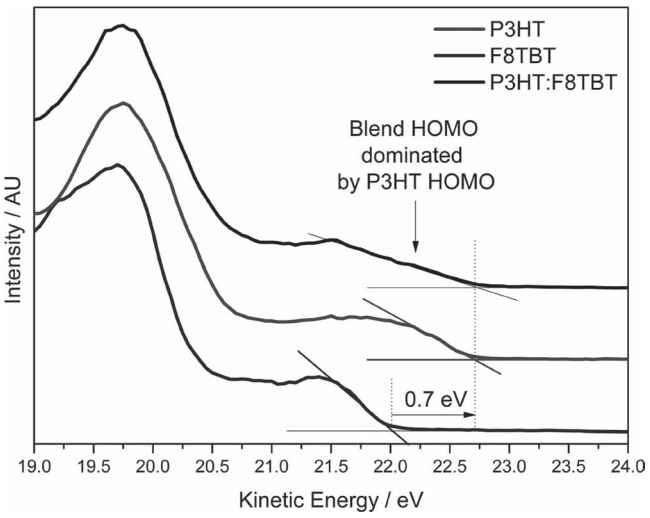

Figure 4. UPS spectra collected on P3HT, F8TBT and P3HT:F8TBT.

Although their measurement on post annealed films shows an increase in the amount of F8TBT at the surface, we believe this to be an artifact of their measurement. The authors evaporated Al electrodes on the polymer film prior to annealing and then removed those electrodes to probe the composition with XPS. However, evaporation of Al electrodes creates a several nanometer thick intermixed layer at the top of the film as it has been reported previously.[24,25] Removing the Al electrode will also remove the intermixed layer (as confirmed by no evidence of Al2p XPS signal on films after Al electrode removal) and partly expose the region below the original P3HT overlayer, which accounts for the increase in F8TBT they observe.

2.2. Bulk Composition of P3HT:F8TBT Films

To probe the bulk composition of the P3HT:F8TBT films of thicknesses comparable to those employed in photovoltaic devices, we used an XPS depth profiling technique. This technique combines XPS, which is used to probe the chemical surface composition, with ion gun sputtering to remove thin layers of the film in order to achieve depth resolution. In the past, this technique was successfully used to examine the composition profiles of other polymer blends, such as Poly(3,4-ethylenedioxythiophene):poly(styrenesulfonate) (PEDOT:PSS),[26] polyaniline:poly(2-acrylamido-2-methyl-1-propanesulfonic acid) (PANI:PAAMPSA),[27] and most recently P3HT:PCBM.[18]

In the case of the P3HT:F8TBT blend, the amount of F8TBT can be determined from the N1s spectra, as P3HT does not contain N atoms. One cannot use the S2p spectra to calculate the composition profile directly as both polymers have S atoms in them. **Figure 5**a shows the composition profile of the sample calculated from the N signal. The signal was corrected to account for the 20% mismatch between the theoretical and measured N quantities as determined from the thin film stochiometries. We note, however, that this does not affect the shape of the depth profile, but solely corrects an offset placing the average composition at 50%, as expected from the 1:1 ratio of the blend in solution. In agreement with our observations from the XPS and UPS measurements on thin films, the top surface of the film is P3HT rich. Underneath the P3HT rich surface layer, an F8TBT rich phase appears. The P3HT concentration then reaches a constant value and remains constant up to the interface with the substrate.

The composition profile we obtained shows a ~70 nm wavelength compositional density wave originating from the air-film interface. We do no observe such a wave originating from the bottom ZnO electrode, as it appears to be a 'neutral surface', which does not preferentially attract either of the polymers. The presence of such a density wave might be due to several reasons. It could provide evidence for spinodal decomposition in the bulk of the polymer:polymer film. Alternatively, it might be a result of the varying kinetics of solvent evaporation during the spin-coating procedure. It has been previously shown that xylene-processed P3HT:F8TBT films show general smoothness as measured by AFM and are expected to produce a finer morphology than that of PFB:F8BT films.[23] This observation is consistent with the possibility of spinodal decomposition, which would result in smooth films. Figure 5b schematically illustrates the sample composition.

2.3. Blend Morphology at the P3HT:F8TBT/ZnO interface

Our XPS depth profiling measurements have revealed that the composition at the bottom interface of the blend film is corresponding to a ~ 1:1 ratio of P3HT to F8TBT. To probe the morphology at this interface, the films were released from the substrate by etching the underlying ZnO film. **Figure 6** shows AFM micrographs taken on P3HT:F8TBT films that were released from the substrate showing the once buried interface

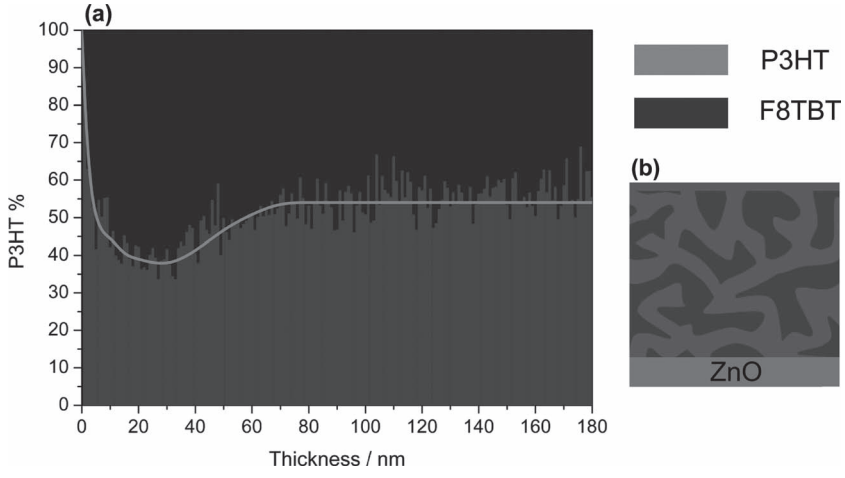

Figure 5. a) XPS depth profile obtained on ~180 nm thick P3HT:F8TBT film on ZnO, b) Schematically shown sample composition.

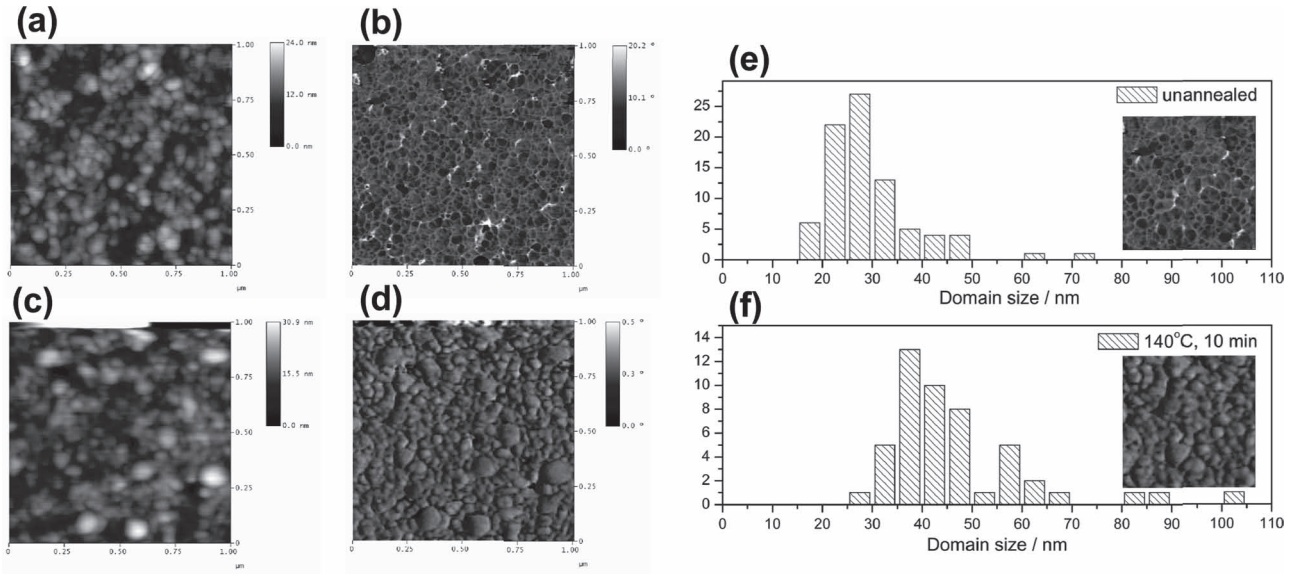

Figure 6. a) AFM height and b) phase images of non-annealed P3HT:F8TBT film released from the ZnO substrate (1 μm × 1 μm). c) AFM height and d) phase images of P3HT:F8TBT film annealed at 140 °C prior to the release from the ZnO substrate (1 μm × 1 μm). e) Histogram of the feature size calculated for the area in the inset (500 nm × 500 nm) for the non-annealed films. f) Histogram of the feature size calculated for the area in the inset (500 nm × 500 nm) for the films annealed at 140 °C.

with ZnO. Figure 6a and b show the height and phase images taken on unannealed P3HT:F8TBT films. The surface consists of small domains, which is particularly evident from the phase image. We note that we cannot distinguish between P3HT and F8TBT domains, however the ratio between the two polymers at this interface is 1:1, as mentioned above. For unannealed films, from a histogram done on the image in the inset of Figure 6e, we find the average domain size of 27.5 nm. McNeill et al have reported 25 nm typical domain size for P3HT:F8TBT blends annealed at 100 °C measured by means of GISAXS.[28] No significant morphological changes are expected for an annealing temperature of 100 °C, so we find these results to be in good agreement with our AFM measurements.

Figure 6c and 6d show the height and phase images of P3HT:F8TBT films annealed at 140 °C. We observe a small increase in the typical feature size at the surface. The histogram in Figure 6f shows that the typical domain size increases to 40.4 nm. This is significantly smaller than the domain size reported by McNeill et al for this annealing temperature.[18] The authors report a typical domain size of 100 nm for annealing temperature of 140 °C, yet this appears to disagree with their observation of the photovoltaic performance being optimal upon annealing at 140 °C. Since the typical exciton diffusion length in polymer blends is estimated to be 10–15 nm, it seems unlikely that a device with a typical domain size of 100 nm would perform best. We find our typical domain size to be much more agreeable to the optimal photovoltaic performance at this annealing temperature.

This slight increase in the typical domain size is also in agreement with previous photoluminescence (PL) spectroscopy measurements[23] which show no increase in PL upon annealing at 140 °C. This is consistent with reorganization of P3HT, rather than significant changes in the degree of phase separation. This reorganization in P3HT is confirmed by UV–vis measurements (see Supporting Information) which show increase in the P3HT shoulder at ~600 nm which is attributed to an increase in P3HT crystallinity.

Interestingly, the typical domain size we measure in the AFM images is in very good agreement to the domain size predicted from the spinodal decomposition in the blend. Assuming the wavelength of the spinodal decomposition in the bulk is equal to the one we observe for the surface directed wave, the typical domain size should be $\sim\lambda/2 \approx 35$ nm, which is in excellent agreement to the 40.4 nm value we calculated from the AFM images.

2.4. Photovoltaic Performance

Figure 7 shows the EQE and *J*–*V* curves measured on as-spun and annealed (140 °C) 480 nm thick P3HT:F8TBT photovoltaic devices. This active layer thickness has been reported to result in optimal photovoltaic device performance in the case of inverted architecture devices.[28] We observe an increase in the EQE of the device upon annealing from 17.3% to 21.2% at 510 nm. The *J*–*V* curves reveal an increase of 50% in the J_{SC} measured under AM 1.5G solar simulator illumination. There is no change in the V_{OC} or the Fill Factor (FF) upon annealing. The photovoltaic performance parameters are summarized in **Table 2**.

We interpret this improvement in the photovoltaic performance to result from improved transport properties of the annealed films. Charge transport is particularly relevant for P3HT:F8TBT blends, as in imbalance in electron and hole mobility is restricting their performance.[29] It has been reported

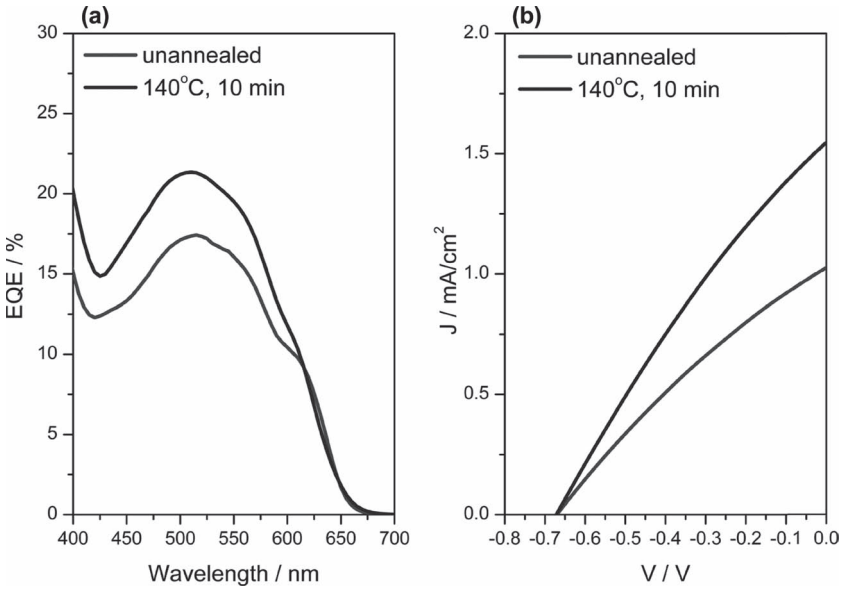

Figure 7. a) EQE of non-annealed and annealed at 140 °C thick inverted architecture PV devices with P3HT:F8TBT active layers. b) *J–V* curves measured under the solar simulator.

that the hole mobility in P3HT increases by an order of magnitude upon annealing,[23] increasing the geminate pair dissociation rate. We note that He et al.[30] observe improved photovoltaic performance for devices with a typical feature size of 25 nm over those of 40 nm, yet it is important to mention that all the devices in that work were annealed and the domain size was mechanically imposed by a nanoimprinting process.

3. Conclusions

In summary, we have investigated the composition and morphology in P3HT:F8TBT blends that have been used for efficient photovoltaic devices. XPS on thin films of pure polymer and the polymer blend show good agreement with the calculated atomic percentage compositions. We find evidence of a thin P3HT surface enrichment layer by means of UPS and ARXPS. Depth profiling measurements reveal a density wave originating from the top surface and a 1:1 P3HT:F8TBT composition ratio at the bottom interface with ZnO. At that interface, the typical domain size as measured by AFM is found to rise slightly upon annealing, showing only a small change in the degree of phase separation. The photovoltaic performance increase is therefore attributed to result from improved P3HT crystallinity in the annealed films, rather than changes in phase separation. Our results contribute to the understanding of phase separation and morphology in this highly efficient polymer:polymer photovoltaic system required to further control them, for example by modifying the substrate surface,[31] the use of solvent additives[32] or by employing a solvent annealing step.

Table 2. V_{OC}, J_{SC}, FF and power conversion efficiency (PCE) of non-annealed and annealed at 140 °C thick inverted architecture PV devices with P3HT:F8TBT active layers under AM1.5 solar simulator conditions (100 mW/cm^2).

	J_{SC} (mA/cm^2)	V_{OC} (V)	FF (%)	PCE (%)
unannealed	1.01	0.66	30.9	0.206
140 °C, 10 minutes	1.54	0.67	29.5	0.305

4. Experimental Section

Sample and Device Fabrication Procedures: Patterned ITO substrates were sonicated in acetone (15 minutes) and 2-propanol (15 minutes) consecutively. Thin films of ZnO were deposited by means of spray pyrolysis deposition (SPD) from a 80g/L zinc acetate dihydrate (Fluka) in methanol solution.[33] The samples were annealed at 350 °C in air for 15 minutes. For the ultraviolet photoemission spectroscopy (UPS) studies, the P3HT (Rieke Metals, M_w = 50-60 kg/mol, RR = 92-93%) and F8TBT (Cambridge Display Technology, M_w = 434 kg/mol) were weighed in air and dissolved in xylene at 70 °C to spin-coat thin films (~5 nm) of P3HT, F8TBT and P3HT:F8TBT 1:1 wt-ratio blends. A 30 mg/mL solution was used to spin coat a ~180 nm thick film (Dektak 6M profilometer) for X-ray Photoemission Spectroscopy (XPS) depth profiling studies (4500 rpm for 60 seconds) and a ~480 nm thick film for photovoltaic devices (1000 rpm for 60 seconds).

Photoemission Spectroscopy: The PES samples were annealed at 140 °C for 10 minutes and transferred to the ultrahigh vacuum (UHV) chamber (ESCALAB 250Xi) for UPS/XPS measurements. The PV samples were transferred to a thermal evaporation chamber for WO_3 (10 nm), Ag (30 nm) and Al (60 nm) deposition under high vacuum (1×10^{-6} mbar). Finally, the samples were post annealed at 140 °C for 10 minutes. UPS measurements were performed using a double-differentially pumped gas discharge lamp emitting He I radiation ($h\nu$ = 21.22 eV) of a He discharge lamp under UHV. XPS measurements were carried out using a XR6 monochromated X-ray source with a 650 μm spot size. Typically the hydrocarbon C1s line at 284.8 eV is used for energy referencing. An Ar+ ion gun was used for sputtering experiments at an ionization energy of 500 eV. The XPS spectra were collected from an area of 300 μm^2 on the substrate. The sputtering rate was estimated to be approximately 1 nm/min. These experiments were carried out at ThermoFisher Scientific, East Grinstead, UK. Angle resolved X-ray photoemission spectroscopy (ARXPS) measurements were carried out in a Kratos AXIS Ultra UHV system. Monochromatic Al Kα line ($h\nu$ = 1486.6 eV) was used for XPS measurements taken at angles of 0°, 15°, 30°, 45° and 60°. This experiment was carried out at Kratos Analytical, Manchester, UK.

Atomic Force Microscopy: AFM was performed in tapping mode using a Digital Instruments Nanoscope IIIa microscope. Films for AFM were prepared on ZnO-coated ITO substrates prepared in identical fashion to those prepared for device fabrication. The films were released from the ZnO substrate by selective etching of the ZnO using HCl.

Photovoltaic Performance Characterization: For External Quantum Efficiency (EQE) measurements (in air) a 250 W tungsten halogen lamp and an Oriel Cornerstone 130 monochromater were used. The measurements were performed as a function of wavelength at intensities ~1 mW/cm^2. To measure the *J–V* curve of the device under AM1.5 conditions, an ABET Solar 2000 solar simulator was used. In order to obtain reliable data, a spectral mismatch correction is carried out using a calibrated and certified inorganic solar cell.

Acknowledgements

We kindly acknowledge A. Wright at Thermo Fisher and S. Hutton at Kratos for their help with the photoemission spectroscopy measurements. T. J. K. B. would like to thank the Engineering and Physical Sciences Research Council (EPSRC) of the United Kingdom for support under grant no. EP/E051804/1. We also thank B. Friedel, C. R. McNeill and U. Steiner for fruitful discussions.

Received: December 12, 2011
Revised: January 31, 2012
Published online: March 19, 2012

[1] R. N. Marks, J. J. M. Halls, D. D. C. Bradley, R. H. Friend, A. B. Holmes, *J. Phys.: Condens. Matter* **1994**, *6*, 1379.
[2] G. Yu, C. Zhang, A. J. Heeger, *Appl. Phys. Lett.* **1994**, *64*, 1540.
[3] W. Ma, C. Yang, X. Gong, K. Lee, A. J. Heeger, *Adv. Funct. Mater.* **2005**, *15*, 1617.
[4] J. Peet, J. Y. Kim, N. E. Coates, W. L. Ma, D. Moses A. J. Heeger, *Nat. Mater.* **2007**, *6*, 497.
[5] J. Y. Kim, K. Lee, N. E. Coates, D. Moses, T.-Q. Nguyen, M. Dante, A. J. Heeger, *Science* **2007**, *317*, 222.
[6] C. H. Woo, P. M. Beaujuge, T. W. Holcombe, O. P. Lee, J. M. J. Frechet, *J. Am. Chem. Soc.* **2010**, *132*, 15547.
[7] H. J. Snaith, R. H. Friend, *Thin Solid Films* **2004**, *451*, 567.
[8] C. R. McNeill, A. Abrusci, J. Zaumseil, R. Wilson, M. J. McKiernan, J. H. Burroughes, J. J. M. Halls, N. C. Greenham, R. H. Friend, *Appl. Phys. Lett.* **2007**, *90*, 193506.
[9] T. W. Holcombe, C. H. Woo, D. F. J. Kavulak, B. C. Thompson, J. M. J. Frechet, *J. Am. Chem. Soc.* **2009**, *131*, 14160.
[10] T. J. K. Brenner, C. R. McNeill, *J. Phys. Chem. C* **2011**, *115*(*39*), 19364.
[11] Y. Xia, R. H. Friend, *Macromolecules* **2005**, *38*, 6466.
[12] A. C. Arias, J. D. MacKenzie, R. Stevenson, J. J. M. Halls, M. Inbasekaran, E. P. Woo, D. Richards, R. H. Friend, *Macromolecules* **2001**, *34*, 6005–6013.
[13] E. Zhuo, J. Cong, Q. Wei, K. Tajima, C. Yang, K. Hashimoto, *Angew. Chem. Int. Ed.* **2011**, *50*, 2799.
[14] S. C. Veenstra, J. Loos, J. M. Kroon, *Prog. Photovolt: Res. Appl.* **2007**, *15*, 727.
[15] S. Y. Heriot, R. A. L. Jones, *Nat. Mater.* **2005**, *4*, 782.
[16] J. T. Rogers, K. Schmidt, M. F. Toney, E. J. Kramer, G. C. Bazan, *Adv. Mater.* **2011**, *23*, 20, 2284.
[17] S. Swaraj, C. Wang, H. Yan, B. Watts, J. Lüning, C. R. McNeill, H. Ade, *Nano Lett.* **2010**, *10*, 2863.
[18] C. R. McNeill, A. Abrusci, I. Hwang, M. A. Ruderer, P. Müller-Buschbaum, N. C. Greenham, *Adv. Funct. Mater.* **2009**, *19*, 3103.
[19] Y. Vaynzof, D. Kabra, L. Zhao, L. L. Chua, U. Steiner, R. H. Friend, *ACS Nano* **2011**, *5*, 329.
[20] A. Kahn, N. Koch, W. Gao, *J. Polym. Sci., Part B: Polym. Phys.* **2003**, *41*, 2529.
[21] B. Friedel, C. R. McNeill, N. C. Greenham, *Chem. Mater.* **2010**, *22*, 3389.
[22] Z.-L. Guan, J. B. Kim, H. Wang, C. Jaye, D. A. Fischer, Y.-L. Loo, A. Kahn, *Org. Electron.* **2010**, *11*, 1779.
[23] C. R. McNeill, J. J. M. Halls, R. Wilson, G. L. Whiting, S. Berkebile, M. G. Ramsey, R. H. Friend, N. C. Greenham, *Adv. Funct. Mater.* **2008**, *18*, 16, 2309.
[24] D. Chen, A. Nakahara, D. Wei, D. Nordlund, T. P. Russell, *Nano Lett.* **2011**, *11*, 561.
[25] C. Y. Nam, D. Su, C. T. Black, *Adv. Funct. Mater.* **2009**, *19*, 1.
[26] J. Hwang, F. Amy, A. Kahn, *Organic Electronics* **2006**, *7*, 387.
[27] J. E. Yoo, W. P. Krekelberg, Y. Sun, J. D. Tarver, T. M. Truskett, Y.-L. Loo, *Chem. Mater* **2009**, *21*, 1948.
[28] T. J. K. Brenner, I. Hwang, N. C. Greenham, C. R. McNeill, *J. Appl. Phys.* **2010**, *107*, 114501.
[29] C. R. McNeill, N. C. Greenham, *Appl. Phys. Lett.* **2010**, *93*, 203310.
[30] X. He, F. Gao, G. Tu, D. Hasko, S. Huttner, U. Steiner, N. C. Greenham, R. H. Friend, W. T. S. Huck, *Nano Lett.* **2010**, *10*, 1302.
[31] Y. Vaynzof, D. Kabra, L. Zhao, P. K. H. Ho, A. T.-S. Wee, R. H. Friend, *Appl. Phys. Lett.* **2010**, *97*, 033309.
[32] M. C. Gwinner, T. J. K. Brenner, C. R. McNeill, J. K. Lee, C. Newby, C. K. Ober, C. R. McNeill, H. Sirringhaus, *J. Mater. Chem.* **2012**, *22*, 4436.
[33] P. M. K. Ratheesh, C. S. Kartha, K. P. Vijaykumar, F. Singh, D. K. Avasthi, *Mater. Sci. Eng. B* **2005**, *117*, 307.